International Journal of Innovative Computing, Information and Control
Volume **14**, Number **5**, October **2018**

ICIC International ©2018 ISSN 1349-4198
pp. 1725–1739

THREE-DIMENSIONAL ADAPTIVE DYNAMIC SURFACE GUIDANCE LAW AGAINST MANEUVERING TARGETS WITH INPUT CONSTRAINTS AND SECOND-ORDER DYNAMICS AUTOPILOT

Lijing Wang[1], Weizhi Jin[2] and Guiying Li[1,*]

[1]School of Mechanical and Electrical Engineering
Heilongjiang University
No. 74, Xuefu Street, Harbin 150001, P. R. China
wanglj_1972@163.com; *Corresponding author: liguiying@hlju.edu.cn

[2]Harbin Power Bureau
No. 267, Xinyang Street, Harbin 150001, P. R. China
jwzh1973@163.com

Received January 2018; revised May 2018

Abstract. *This paper conducts the related researches about the guidance strategy of missile against maneuvering targets subject to impact angle constraints, input constraints and missile autopilot. Firstly, the three-dimensional guidance system model is established, which has the impact angle constraints, input constraints and missile autopilot. Secondly, an adaptive dynamic surface guidance (ADSG) strategy with impact angle constraints, autopilot lag and input constraints is designed based on the dynamic surface method, sliding mode control, sliding mode filter and adaptive technology. In order to deal with the problem of input constraints, the auxiliary system is introduced. Meanwhile, a new adaptive algorithm is proposed to reduce the tracking error of the sliding mode filter which can further improve the guidance performance of the system. Finally, Lyapunov theory is adopted to prove that the states of the closed-loop system are uniformly ultimately bounds. By conducting the numerical simulations, the effectiveness of the proposed guidance law can be proved.*

Keywords: Three-dimensional guidance law, Second-order dynamics of missile autopilot, Input constraints, Adaptive control, Dynamic surface control

1. **Introduction.** With the development of modern aircraft design technology, the maneuver power of attacking targets is constantly increasing. The strong robust terminal guidance law with intercepting the high-speed maneuvering targets is designed, which can guarantee to intercept the precise target of missiles. Usually, the miss distance and specific terminal impact angle at the moment of the terminal are satisfied simultaneously [1].

In recent years, domestic and foreign experts and scholars in the control field have conducted a considerable amount of researches and explorations in the guidance technology of missile. In [2,3], the guidance law was designed which has terminal impact angle, but it just intercepts non-maneuvering target. In order to intercept highly manoeuverable target, a circular guidance law with attack angle constraints is designed in [4,5]. It is well known that the sliding mode control has good robustness to external disturbances; therefore, it is used widely in the control field [6-8]. In [7], a chattering free sliding mode controller was designed for attitude model based on sliding mode control and backstepping control. In [8], a fast terminal sliding mode guidance law with impact angle was designed for two dimensional guidance model based on nonlinear disturbance observer and

DOI: 10.24507/ijicic.14.05.1725

terminal sliding mode control theory. Due to the dynamic of the missile autopilot which must be considered in the actual design process of guidance system, it leads to a certain time delay between the guidance command signal and the deflection signal of the control rudder. Thus, the delay property of the autopilot always has significant influence on the aspect of guidance precision. In [9,10], a sliding mode guidance law was proposed for the guidance system with first-order dynamics of missile autopilot. As the intercept process of target and missile happens in the three-dimensional space and consider the guidance system mode of three-dimensional with the second-order dynamic of missile autopilot, an adaptive guidance law with terminal impact angle was proposed in [11,12]. In order to enhance the guidance system's robustness, using the observer, a dynamic surface sliding mode three-dimensional guidance strategy was designed with terminal impact angle for guidance system subject to the second-order dynamic of missile autopilot in [13,14].

At present, during the process of actual design system, most of documents did not consider the actual physical limitations of actuators and the control force provided by the actuators is limited [15,16]. In [16], an adaptive robust control scheme was proposed for cubesats with external disturbances, which can deal with input saturation problem by the use of the adaptive dynamic neural network. Some guidance law designs have not considered the input constraints; however, the problem of actuator saturation may emerge in the practical actuation. It is obvious that this problem will result in the system guidance performance weakness, or even the guidance system instability. Therefore, the guidance law with acceleration saturation constraint is studied having significant significance theoretically and practically. In [17], the three-dimensional sliding mode guidance laws were proposed for hypersonic vehicle with external disturbances and input saturation based on sliding mode control method and adaptive method, which used the hyperbolic tangent function and auxiliary system to solve the input saturation problem. In [18,19], an ADSG law was designed with autopilot of missile and acceleration constraint. In [20,21] by using hyperbolic tangent function, adaptive technology and dynamic surface method, an ADSG law subject to acceleration constraint was designed; however, only the first order dynamic of the missile autopilot was considered. A three-dimensional (3D) ADSG law was proposed for guidance system in presence of missile autopilot's second-order dynamics and acceleration constraint; however, the terminal impact angle was not considered in [23].

In order to further solve guidance problem of missiles against maneuvering targets which subjects to impact angle constraints, input constraints and missile autopilot with second-order dynamics, a 3D ADSGL is designed on the basis of the low filtering and adaptive control theory in this paper. The guidance scheme can be able to impact angle constraints, input constraints and dynamics of missile autopilot at the same time. Compared with the literature listed above, this paper has innovative aspects as the following.

(1) An improved 3D-ADSGL is proposed without differentiation of the virtual controllers, and the adaptive algorithm is introduced to compensate the effect of the error caused by the sliding mode filter, which can improve the guidance performance.

(2) The auxiliary system is introduced to deal with input constraints. Compared with [11,12], the input constraints are taken into account.

(3) Compared with [19,20], this paper takes missile autopilot with second-order dynamics into consideration, which have practical significance about the designed controller.

The rest of this article is as follows. In Section 2, guidance model in 3D space is established. In Section 3, an adaptive dynamic surface guidance law is proposed, where the proofs of the system stability are also given. In Section 4, the efficiency of the proposed guidance can be confirmed laws through the results of the presented simulation. Section 5 concludes this paper.

2. **Preliminaries.** In this section, for the three-dimensional guidance system, the target-missile relative motion equations are presented. Figure 1 shows a 3D interception geometry. T represents the target; M denotes the missile; $Mxyz$ expresses the inertial reference frame; $Mx_4y_4z_4$ is a line-of-sight (LOS) frame; r is the relative distance between the target and missile; q_ε and q_β are the elevation and azimuth angles of the LOS, respectively.

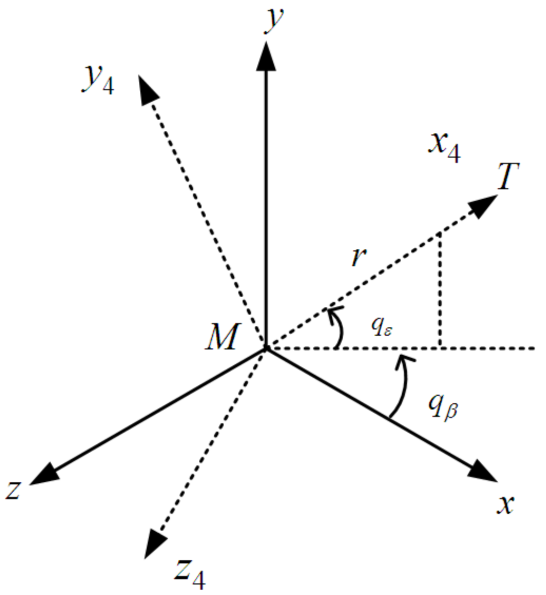

FIGURE 1. Three-dimensional interception geometry

According to the kinematics principle, the three-dimensional relative motion dynamics between the missile and the target can be represented by the following differential equations [21]

$$\ddot{r} - r\dot{q}_\varepsilon^2 - r\dot{q}_\beta^2 \cos^2 q_\varepsilon = a_{Tr} - a_{Mr} \tag{1}$$

$$r\ddot{q}_\varepsilon + 2\dot{r}\dot{q}_\varepsilon + r\dot{q}_\beta^2 \sin q_\varepsilon \cos q_\varepsilon = a_{T\varepsilon} - a_{M\varepsilon} \tag{2}$$

$$-r\ddot{q}_\beta \cos q_\varepsilon - 2\dot{r}\dot{q}_\beta \cos q_\varepsilon + 2r\dot{q}_\varepsilon\dot{q}_\beta \sin q_\varepsilon = a_{T\beta} - a_{M\beta} \tag{3}$$

relative motion can be seen from Figure 1, where $\boldsymbol{a}_M = [a_{Mr}, a_{M\varepsilon}, a_{M\beta}]^{\mathrm{T}}$ is the vectors of the missile's acceleration and $\boldsymbol{a}_T = [a_{Tr}, a_{T\varepsilon}, a_{T\beta}]^{\mathrm{T}}$ is the vectors of the target's acceleration in the LOS frame.

The following second-order dynamics [11] can approximately express the autopilot dynamics of the missile

$$\ddot{a}_{M\varepsilon} = -2\xi\omega_n\dot{a}_{M\varepsilon} - \omega_n^2 a_{M\varepsilon} + \omega_n^2 u_\varepsilon + d_\varepsilon \tag{4}$$

$$\ddot{a}_{M\beta} = -2\xi\omega_n\dot{a}_{M\beta} - \omega_n^2 a_{M\beta} + \omega_n^2 u_\beta + d_\beta \tag{5}$$

where ξ is the damping ratio, ω_n denotes the undamped natural frequency, and d_ε and d_β denote uncertainties in this model. u_ε and u_β are the missile acceleration commands.

Let $q_{\varepsilon d}$ and $q_{\beta d}$ be pre-specified with a constant value. Also state variables are defined as $\boldsymbol{x}_1 = [q_\varepsilon - q_{\varepsilon d}, q_\beta - q_{\beta d}]^{\mathrm{T}}$, $\boldsymbol{x}_2 = [\dot{q}_\varepsilon, \dot{q}_\beta]^{\mathrm{T}}$, $\boldsymbol{x}_3 = [a_{M\varepsilon}, a_{M\beta}]^{\mathrm{T}}$ and $\boldsymbol{x}_4 = [\dot{a}_{M\varepsilon}, \dot{a}_{M\beta}]^{\mathrm{T}}$, and then (1)-(5) can be expressed as follows:

$$\begin{cases} \dot{\boldsymbol{x}}_1 = \boldsymbol{x}_2 \\ \dot{\boldsymbol{x}}_2 = \boldsymbol{f}(\boldsymbol{x}_1, \boldsymbol{x}_2) + \boldsymbol{b}\boldsymbol{x}_3 + \boldsymbol{d}_1 \\ \dot{\boldsymbol{x}}_3 = \boldsymbol{x}_4 \\ \dot{\boldsymbol{x}}_4 = -\omega_n^2\boldsymbol{x}_3 - 2\xi\omega_n\boldsymbol{x}_4 + \omega_n^2 \mathrm{sat}(\boldsymbol{u}) + \boldsymbol{d}_2 \end{cases} \tag{6}$$

where

$$\boldsymbol{f}(\boldsymbol{x}_1,\boldsymbol{x}_2)=\begin{bmatrix} -\dfrac{2\dot{R}}{R}\dot{q}_\varepsilon-\dot{q}_\beta^2\sin q_\varepsilon\cos q_\varepsilon \\ -\dfrac{2\dot{R}}{R}\dot{q}_\beta+2q_\varepsilon q_\beta\tan q_\varepsilon \end{bmatrix},\ \boldsymbol{b}=\begin{bmatrix} -\dfrac{1}{R} & 0 \\ 0 & \dfrac{1}{R\cos q_\varepsilon} \end{bmatrix},$$

$$\boldsymbol{d}_1=\begin{bmatrix} \dfrac{a_{T\varepsilon}}{R} \\ -\dfrac{a_{T\beta}}{R\cos q_\varepsilon} \end{bmatrix},\ \boldsymbol{d}_2=\begin{bmatrix} d_\varepsilon \\ d_\beta \end{bmatrix},$$

$\mathrm{sat}(\boldsymbol{u})$ can be described as follows

$$\mathrm{sat}(\boldsymbol{u})=[\mathrm{sat}(u_\varepsilon),\mathrm{sat}(u_\beta)]^{\mathrm{T}}$$
$$\mathrm{sat}(u_i)=\begin{cases} u_{\max}, & u_i\geq u_{\max} \\ u_i, & -u_{\max}<u_i<u_{\max}\ , \quad i=\varepsilon,\beta \\ -u_{\max}, & u_i\leq -u_{\max} \end{cases} \tag{7}$$

where $u_{\max}$ is the known upper bound for control input.

The following assumption and lemma are useful to design the three dimension terminal guidance law.

Assumption 2.1. *In system (6), $\boldsymbol{d}_1$ and $\boldsymbol{d}_2$ represent the lumped external disturbances and the autopilot uncertainties, respectively. They are assumed to be bounded and they can satisfy the following condition*

$$\|\boldsymbol{d}_1\|\leq d_{1M},\quad \|\boldsymbol{d}_2\|\leq d_{2M} \tag{8}$$

where d_{1M} and d_{2M} are unknown positive constants.

Lemma 2.1. [24]. *The first-order sliding mode differentiator is designed as the following differential equations*

$$\begin{cases} \dot{\varsigma}_0=-\mu_0\left|\varsigma_0-l(t)\right|^{0.5}\mathrm{sign}\left(\varsigma_0-l(t)\right)+\varsigma_1 \\ \dot{\varsigma}_1=-\mu_1\mathrm{sign}\left(\varsigma_1-\varsigma_0\right) \end{cases} \tag{9}$$

where ς_1 and ς_0 are the states of the system (9), and μ_0 and μ_1 are the designed parameters. After a finite time, then $\dot{\varsigma}_0$ can approximate the differential term $\dot{l}(t)$ to an arbitrary accuracy if the initial deviations $\varsigma_0-l(t)$ and $\dot{\varsigma}_0-\dot{l}(t)$ are bounded [19].

An adaptive dynamic surface three dimension terminal guidance law is designed for the guidance system (6), which has the consideration of impact angle constraints, input constraints and missile autopilot with second-order dynamics. The LOS angle error $\boldsymbol{x}_1$ and the LOS angular rate $\boldsymbol{x}_2$ can be guaranteed to converge to small region around zero in finite time by this guidance law.

3. **Main Results.** On the basis of the dynamic surface control, adaptive technique and auxiliary system, a robust dynamic surface sliding mode guidance scheme is designed for the three-dimensional guidance system (6). The proposed guidance scheme not only takes advantage of the sliding mode filter to avoid the differential of the virtual control signals, but also introduces the adaptive law to compensate the effect of the error caused by sliding mode filter. The specific process is as follows.

Step 1: In order to make the system states $\boldsymbol{x}_1$ and $\boldsymbol{x}_2$ approach to zero fast in finite time along the sliding mode surface, the non-singular fast terminal sliding surface is designed as follows

$$\boldsymbol{s}_2=\boldsymbol{x}_2+\frac{\alpha_1}{\alpha_0}\left(\exp(\alpha_0\left|\boldsymbol{x}_1\right|)-1\right)\mathrm{sign}\left(\boldsymbol{x}_1\right)+\boldsymbol{\alpha}_2\boldsymbol{\beta}(\boldsymbol{x}_1) \tag{10}$$

$$\boldsymbol{\beta}(x_1) = [\beta(x_{11}), \beta(x_{12})]^{\mathrm{T}}$$

$$\beta(x_{1i}) = \begin{cases} \mathrm{sig}(x_{1i})^{\lambda}, & |x_{1i}| > \eta \\ \dfrac{r_1}{\alpha_0}\left(\exp(\alpha_0 |x_{1i}|) - 1\right) \mathrm{sign}\,(x_{1i}) + r_2 \mathrm{sign}(x_{1i})\,(x_{1i})^2, & |x_{1i}| \le \eta \end{cases} \quad (i = 1, 2) \tag{11}$$

$$r_1 = (2 - \lambda)\eta^{\lambda - 1} \tag{12}$$

$$r_2 = (\lambda - 1)\eta^{\lambda - 2} \tag{13}$$

where $\mathrm{sig}(\cdot)^{\lambda} = |\cdot|^{\lambda}\mathrm{sign}(\cdot)$, $0 < \lambda < 1$, $\mathrm{sign}(\cdot)$ denotes the signum function, and α_0, α_1, α_2 and η are positive constants.

The differential of $\boldsymbol{s}_2$ can be written as

$$\dot{\boldsymbol{s}}_2 = \boldsymbol{f}(\boldsymbol{x}_1, \boldsymbol{x}_2) + \boldsymbol{b}\boldsymbol{x}_3 + \boldsymbol{d}_1 + \alpha_1 \exp\left(\alpha_0 |\boldsymbol{x}_{1i}|\right) \boldsymbol{x}_2 + \alpha_2 \dot{\boldsymbol{\beta}}(\boldsymbol{x}_1) \tag{14}$$

Define the virtual control functions $\boldsymbol{x}_3^*$ as

$$\boldsymbol{x}_3^* = \boldsymbol{b}^{-1}\left[-\boldsymbol{f}(\boldsymbol{x}_1, \boldsymbol{x}_2) - \alpha_1 \exp\left(\alpha_0 |\boldsymbol{x}_{1i}|\right) \boldsymbol{x}_2 - \alpha_2 \dot{\boldsymbol{\beta}}(\boldsymbol{x}_1) - k_2 \boldsymbol{s}_2 - k_1 \mathrm{sig}(\boldsymbol{s}_2)^{\gamma} - \frac{\boldsymbol{s}_2}{4\varepsilon_1}\right] \tag{15}$$

where k_1, k_2 and ε_1 are positive constants.

To avoid multiple differentiation of $\boldsymbol{x}_3^*$, the first-order sliding mode differentiator is introduced to estimate $\dot{\boldsymbol{x}}_3^*$

$$\begin{cases} \dot{\varsigma}_{10i} = -\mu_{10i} \left|\varsigma_{10} - \boldsymbol{x}_{3i}^*\right|^{0.5} \mathrm{sign}\left(\varsigma_{10i} - \boldsymbol{x}_{3i}^*\right) + \varsigma_{11i} \\ \dot{\varsigma}_{11i} = -\mu_{11i} \mathrm{sign}\left(\varsigma_{11i} - \varsigma_{10i}\right) \end{cases} \tag{16}$$

where ς_{11i} and ς_{10i} are the states of the sliding mode differentiator, and μ_{10i} and μ_{11i} are positive constants.

According to (16) and Lemma 2.1, the inequality is satisfied as

$$|\dot{\boldsymbol{x}}_{3i}^* - \dot{\varsigma}_{10i}| \le \ell_{1i} \tag{17}$$

where ℓ_{1i} can estimate the error of the sliding mode differentiator and satisfy $|\ell_{1i}| \le \bar{\ell}_{1i}$, and $\bar{\ell}_{1i}$ is a positive constant.

Step 2: Define the tracking error variable

$$\boldsymbol{s}_3 = \boldsymbol{x}_3 - \boldsymbol{x}_3^* \tag{18}$$

The time derivative of $\boldsymbol{s}_3$ can be given by

$$\dot{\boldsymbol{s}}_3 = \boldsymbol{x}_4 - \dot{\boldsymbol{x}}_3^* \tag{19}$$

Based on (15), the virtual control law is designed as

$$\boldsymbol{x}_4^* = -k_3 \boldsymbol{s}_3 + \dot{\varsigma}_{10i} - \hat{\ell}_{1i} \tan\left(\frac{s_{3i}}{p_1}\right) - \boldsymbol{b}\boldsymbol{s}_2 \tag{20}$$

where $k_3 > 0$.

In order to reduce the estimation error of the sliding differentiator, an adaptive law is designed as

$$\hat{\ell}_{1i} = \beta_1 s_{3i} \tan\left(\frac{s_{3i}}{p_1}\right) - \varsigma_1 \beta_1 \hat{\ell}_{1i} \tag{21}$$

where p_1, β_1 and ς_1 are positive constants.

To avoid multiple differentiation of $\boldsymbol{x}_4^*$, the first-order sliding mode differentiator is introduced to estimate $\dot{\boldsymbol{x}}_4^*$

$$\begin{cases} \dot{\varsigma}_{20i} = -\mu_{20i} \left|\varsigma_{20i} - \boldsymbol{x}_{4i}^*\right|^{0.5} \mathrm{sign}\left(\varsigma_{20i} - \boldsymbol{x}_{4i}^*\right) + \varsigma_{21i} \\ \dot{\varsigma}_{21i} = -\mu_{21i} \mathrm{sign}\left(\varsigma_{21i} - \varsigma_{20i}\right) \end{cases} \tag{22}$$

where ς_{21i} and ς_{20i} are the states of the sliding mode differentiator, and μ_{20i} and μ_{21i} are positive constants.

From (22) and Lemma 2.1, the inequality is satisfied as

$$|\dot{\boldsymbol{x}}_{4i}^* - \dot{\varsigma}_{20i}| \leq \ell_{2i} \tag{23}$$

where ℓ_{2i} can estimate the error of the sliding mode differentiator and satisfy $|\ell_{2i}| \leq \bar{\ell}_{2i}$, and $\bar{\ell}_{2i}$ is a positive constant.

Step 3: Define the tracking error variable

$$\boldsymbol{s}_4 = \boldsymbol{x}_4 - \boldsymbol{x}_4^* \tag{24}$$

Computing the first order derivative of $\boldsymbol{s}_4$, we obtain

$$\dot{\boldsymbol{s}}_4 = -\omega_n^2 \boldsymbol{x}_3 - 2\zeta\omega_n \boldsymbol{x}_4 + \omega_n^2 \mathrm{sat}(\boldsymbol{u}) + \boldsymbol{d}_2 - \dot{\boldsymbol{x}}_4^* \tag{25}$$

To cope with the input saturation, motivated by the work of [15], the auxiliary system (26) is introduced

$$\dot{\boldsymbol{v}}_u = \begin{cases} -\lambda_1 \boldsymbol{v}_u - \dfrac{\left|w_n^2 \boldsymbol{s}_4^{\mathrm{T}} \Delta \boldsymbol{u}\right| + 0.5 w_n^2 \Delta \boldsymbol{u}^{\mathrm{T}} \Delta \boldsymbol{u}}{\|\boldsymbol{v}_u\|^2} \boldsymbol{v}_u & \|\boldsymbol{v}_u\| \geq \eta_1 \\ -w_n^2 \Delta \boldsymbol{u} - c_1 \mathrm{sig}(\boldsymbol{v}_u)^\gamma - c_2 \mathrm{sign}(\boldsymbol{v}_u), & \\ 0, & \|\boldsymbol{v}_u\| < \eta_1 \end{cases} \tag{26}$$

where λ_1, c_1, $c_2, \eta_1 > 0$, $\Delta \boldsymbol{u} = \mathrm{sat}(\boldsymbol{u}) - \boldsymbol{u}$; $\boldsymbol{v}_u = [v_{u1}, v_{u2}]^{\mathrm{T}}$ is the state variable of the auxiliary system; η_1 is a positive constant.

The guidance law $\boldsymbol{u}$ is defined as

$$\boldsymbol{u} = \frac{1}{w_n^2} \left[\omega_n^2 \boldsymbol{x}_3 + 2\zeta\omega_n \boldsymbol{x}_4 + \dot{\varsigma}_{20} - \ell_{2i} - k_4 \boldsymbol{s}_4 - \boldsymbol{s}_3 - \frac{\boldsymbol{s}_4}{4\varepsilon_2} + \lambda_3 \boldsymbol{v}_u - \frac{1}{2} \frac{\lambda_3^2 \|\boldsymbol{s}_4\|^2 \boldsymbol{s}_4}{\xi^2 + \|\boldsymbol{s}_4\|^2} \right] \tag{27}$$

where $\varepsilon_2 > 0$, k_4, $\lambda_3 > 0$, ξ is defined as

$$\dot{\xi} = \begin{cases} -\lambda_2 \xi - \dfrac{1}{2} \dfrac{\lambda_3^2 \|\boldsymbol{s}_4\|^2 \xi}{\xi^2 + \|\boldsymbol{s}_4\|^2} - c_3 \mathrm{sig}(\xi)^\gamma - c_4 \mathrm{sign}(\xi), & \|\boldsymbol{s}_4\| \geq \eta_2 \\ 0, & \|\boldsymbol{s}_4\| < \eta_2 \end{cases} \tag{28}$$

where λ_2, c_3, c_4 and η_2 are positive constants.

To decrease the estimation error of the sliding differentiator, an adaptive law is designed

$$\dot{\hat{\ell}}_{2i} = \beta_2 s_{4i} \tan\left(\frac{s_{4i}}{p_2}\right) - \varsigma_2 \beta_2 \hat{\ell}_{2i} \tag{29}$$

where p_2, β_2 and ς_2 are positive constants.

Theorem 3.1. *For the guidance system (6) with Assumption 2.1, under the adaptive dynamic surface guidance law (26)-(28) and adaptive law (21) and (29), the state of closed-loop system is regulated. The following conclusions can be obtained.*

(1) The $\boldsymbol{s}_i$ will converge to the region Δ_i in finite time

$$\|\boldsymbol{s}_i\| \leq \Delta_i \tag{30}$$

(2) The $\boldsymbol{x}_1$ will converge to the region $|x_{1i}| \leq \Delta_{x_{1i}}$ and $\boldsymbol{x}_2$ will converge to the region $|x_{2i}| \leq \Delta_{x_{2i}}$ in finite time

$$|x_{1i}| \leq \Delta_{x_{1i}} = \max\left\{\eta, \min\left\{\frac{1}{\alpha_0} \ln \frac{\alpha_0 \Delta_i + \alpha_1}{\alpha_1}, \left(\frac{\Delta_i}{\alpha_2}\right)^\gamma \right\}\right\} \tag{31}$$

$$|x_{2i}| \leq \Delta_{x_{2i}} = \Delta x_{1i} + \frac{\alpha_1}{\alpha_0} \left(\exp(\alpha_0 \Delta x_{1i}) - 1\right) + \alpha_2 \mathrm{sig}\left(\Delta x_{1i}\right)^\gamma \tag{32}$$

where x_{1i} and x_{2i} are the ith component of vectors $\boldsymbol{x}_1$ and $\boldsymbol{x}_2$.

Proof: Choose Lyapunov function as

$$V_1 = \frac{1}{2}\boldsymbol{s}_2^{\mathrm{T}}\boldsymbol{s}_2 + \frac{1}{2}\boldsymbol{s}_3^{\mathrm{T}}\boldsymbol{s}_3 + \frac{1}{2}\boldsymbol{s}_4^{\mathrm{T}}\boldsymbol{s}_4 + \frac{1}{2}\boldsymbol{v}_u^{\mathrm{T}}\boldsymbol{v}_u + \frac{1}{2\beta_1}\tilde{\ell}_{1i} + \frac{1}{2\beta_2}\tilde{\ell}_{2i} + \frac{1}{2}\xi^2 \tag{33}$$

where $\tilde{\ell}_{1i} = \ell_{1i} - \hat{\ell}_{1i}$, $\tilde{\ell}_{2i} = \ell_{2i} - \hat{\ell}_{2i}$.

Let

$$V_{11} = \frac{1}{2}\boldsymbol{s}_2^{\mathrm{T}}\boldsymbol{s}_2 \tag{34}$$

$$V_{12} = \frac{1}{2}\boldsymbol{s}_3^{\mathrm{T}}\boldsymbol{s}_3 + \frac{1}{2\beta_1}\tilde{\ell}_{1i} \tag{35}$$

$$V_{13} = \frac{1}{2}\boldsymbol{s}_4^{\mathrm{T}}\boldsymbol{s}_4 + \frac{1}{2}\boldsymbol{v}_u^{\mathrm{T}}\boldsymbol{v}_u + \frac{1}{2\beta_2}\tilde{\ell}_{2i} + \frac{1}{2}\xi^2 \tag{36}$$

With the application of (15), time derivative of (34) results in

$$\begin{aligned}
\dot{V}_{11} &= \boldsymbol{s}_2^{\mathrm{T}}\dot{\boldsymbol{s}}_2 \\
&= \boldsymbol{s}_2^{\mathrm{T}}\left(\boldsymbol{b}\boldsymbol{s}_3 + \boldsymbol{d}_1 - k_2\boldsymbol{s}_2 - k_1\mathrm{sig}(\boldsymbol{s}_2)^{\gamma} - \frac{\boldsymbol{s}_2^{\mathrm{T}}\boldsymbol{s}_2}{4\varepsilon_1}\right) \\
&= \boldsymbol{s}_2^{\mathrm{T}}\boldsymbol{b}\boldsymbol{s}_3 - k_2\boldsymbol{s}_2^{\mathrm{T}}\boldsymbol{s}_2 - k_1\boldsymbol{s}_2^{\mathrm{T}}\mathrm{sig}(\boldsymbol{s}_2)^{\gamma} + \boldsymbol{s}_2^{\mathrm{T}}\boldsymbol{d}_1 - \frac{\boldsymbol{s}_2^{\mathrm{T}}\boldsymbol{s}_2}{4\varepsilon_1} \\
&\le \boldsymbol{s}_2^{\mathrm{T}}\boldsymbol{b}\boldsymbol{s}_3 - k_2\boldsymbol{s}_2^{\mathrm{T}}\boldsymbol{s}_2 - k_1\boldsymbol{s}_2^{\mathrm{T}}\mathrm{sig}(\boldsymbol{s}_2)^{\gamma} + \frac{\boldsymbol{s}_2^{\mathrm{T}}\boldsymbol{s}_2}{4\varepsilon_1} + \varepsilon_1 d_{1M}^2 - \frac{\boldsymbol{s}_2^{\mathrm{T}}\boldsymbol{s}_2}{4\varepsilon_1} \\
&\le \boldsymbol{s}_2^{\mathrm{T}}\boldsymbol{b}\boldsymbol{s}_3 - k_2\boldsymbol{s}_2^{\mathrm{T}}\boldsymbol{s}_2 - k_1\boldsymbol{s}_2^{\mathrm{T}}\mathrm{sig}(\boldsymbol{s}_2)^{\gamma} + \varepsilon_1 h_1
\end{aligned} \tag{37}$$

where $h_1 = d_{1M}^2$.

Computing the first order derivative of V_{12} and using (20) and (21), it can be rewritten as

$$\begin{aligned}
\dot{V}_{12} &= \boldsymbol{s}_3^{\mathrm{T}}\dot{\boldsymbol{s}}_3 - \frac{1}{\beta_1}\tilde{\ell}_{1i}\dot{\hat{\ell}}_{1i} \\
&= \boldsymbol{s}_3^{\mathrm{T}}\boldsymbol{s}_4 - k_3\boldsymbol{s}_3^{\mathrm{T}}\boldsymbol{s}_3 - \boldsymbol{s}_3^{\mathrm{T}}\boldsymbol{b}\boldsymbol{s}_2 + \boldsymbol{s}_3^{\mathrm{T}}\left(\dot{\varsigma}_{10i} - \dot{\boldsymbol{x}}_{3i}^{*} - \hat{\ell}_{1i}\tan\left(\frac{s_{3i}}{p_1}\right)\right) \\
&\quad - \frac{1}{\beta_1}\tilde{\ell}_{1i}\left(\beta_1 s_{3i}\tan\left(\frac{s_{3i}}{p_1}\right) - \varsigma_1\beta_1\hat{\ell}_{1i}\right) \\
&\le \boldsymbol{s}_3^{\mathrm{T}}\boldsymbol{s}_4 - k_3\boldsymbol{s}_3^{\mathrm{T}}\boldsymbol{s}_3 - \boldsymbol{s}_3^{\mathrm{T}}\boldsymbol{b}\boldsymbol{s}_2 + s_{3i}\left(\ell_{1i} - \hat{\ell}_{1i}\tan\left(\frac{s_{3i}}{p_1}\right)\right) \\
&\quad - \frac{1}{\beta_1}\tilde{\ell}_{1i}\left(\beta_1 s_{3i}\tan\left(\frac{s_{3i}}{p_1}\right) - \varsigma_1\beta_1\hat{\ell}_{1i}\right) \\
&\le \boldsymbol{s}_3^{\mathrm{T}}\boldsymbol{s}_4 - k_3\boldsymbol{s}_3^{\mathrm{T}}\boldsymbol{s}_3 - \boldsymbol{s}_3^{\mathrm{T}}\boldsymbol{b}\boldsymbol{s}_2 + \ell_{1i}\left|s_{3i}\right| - \ell_{1i}s_{3i}\tan\left(\frac{s_{3i}}{p_1}\right) + \varsigma_1\tilde{\ell}_{1i}\hat{\ell}_{1i}
\end{aligned} \tag{38}$$

As

$$-\ell_{1i}s_{3i}\tan\left(\frac{s_{3i}}{p_1}\right) \le -\frac{\ell_{1i}s_{3i}^2}{|s_{3i}| + p_1}, \quad \tilde{\ell}_{1i}\hat{\ell}_{1i} = \tilde{\ell}_{1i}\left(\ell_{1i} - \tilde{\ell}_{1i}\right) \le \frac{1}{2}\ell_{1i}^2 - \frac{1}{2}\tilde{\ell}_{1i}^2 \tag{39}$$

substituting (39) into (38), one can obtain

$$\begin{aligned}
\dot{V}_{12} &\le \boldsymbol{s}_3^{\mathrm{T}}\boldsymbol{s}_4 - k_3\boldsymbol{s}_3^{\mathrm{T}}\boldsymbol{s}_3 - \boldsymbol{s}_3^{\mathrm{T}}\boldsymbol{b}\boldsymbol{s}_2 + |s_{3i}|\,\ell_{1i} - \frac{\ell_{1i}s_{3i}^2}{|s_{3i}| + p_1} + \frac{\varsigma_1}{2}\ell_{1i}^2 - \frac{\varsigma_1}{2}\tilde{\ell}_{1i}^2 \\
&\le \boldsymbol{s}_3^{\mathrm{T}}\boldsymbol{s}_4 - k_3\boldsymbol{s}_3^{\mathrm{T}}\boldsymbol{s}_3 - \boldsymbol{s}_3^{\mathrm{T}}\boldsymbol{b}\boldsymbol{s}_2 - \frac{\varsigma_1}{2}\tilde{\ell}_{1i}^2 + \frac{\varsigma_1}{2}\ell_{1i}^2
\end{aligned} \tag{40}$$

Computing the first order derivative of V_{13}, one can obtain

$$\begin{aligned}
\dot{V}_{13} &= \boldsymbol{s}_4^{\mathrm{T}}\dot{\boldsymbol{s}}_4 + \boldsymbol{v}_u^{\mathrm{T}}\dot{\boldsymbol{v}}_u + \xi\dot{\xi} - \frac{1}{\beta_2}\tilde{\ell}_{2i}\dot{\hat{\ell}}_{2i} \\
&\le -\boldsymbol{s}_4^{\mathrm{T}}\boldsymbol{s}_3 - k_4\boldsymbol{s}_4^{\mathrm{T}}\boldsymbol{s}_4 + \|\boldsymbol{s}_4\|\,\|\boldsymbol{d}_2\| + \lambda_3\boldsymbol{s}_4^{\mathrm{T}}\boldsymbol{v}_u - \frac{1}{2}\frac{\lambda_3^2\|\boldsymbol{s}_4\|^2\boldsymbol{s}_4^{\mathrm{T}}\boldsymbol{s}_4}{\xi^2+\|\boldsymbol{s}_4\|^2} + w_n^2\boldsymbol{s}_4^{\mathrm{T}}\Delta\boldsymbol{u} \\
&\quad - \frac{\boldsymbol{s}_4^{\mathrm{T}}\boldsymbol{s}_4}{4\varepsilon_2} - \lambda_1\boldsymbol{v}_u^{\mathrm{T}}\boldsymbol{v}_u - \left|w_n^2\boldsymbol{s}_4^{\mathrm{T}}\Delta\boldsymbol{u}\right| - \frac{1}{2}w_n^2\Delta\boldsymbol{u}^{\mathrm{T}}\Delta\boldsymbol{u} - w_n^2\boldsymbol{v}_u^{\mathrm{T}}\Delta\boldsymbol{u} - c_1\boldsymbol{v}_u^{\mathrm{T}}\mathrm{sig}(\boldsymbol{v}_u)^\gamma \\
&\quad - \boldsymbol{s}_4^{\mathrm{T}}\left(\dot{\varsigma}_{20i} - \dot{\boldsymbol{x}}_{4i}^* - \hat{\ell}_{2i}\tan\left(\frac{s_{4i}}{p_2}\right)\right) - \frac{1}{\beta_2}\tilde{\ell}_{2i}\left(\beta_2 s_{4i}\tan\left(\frac{s_{4i}}{p_2}\right) - \varsigma_2\beta_2\hat{\ell}_{2i}\right) \\
&\quad - c_2\boldsymbol{v}_u^{\mathrm{T}}\mathrm{sign}(\boldsymbol{v}_u)\lambda_2\xi^2 - \frac{1}{2}\frac{\lambda_3^2\|\boldsymbol{s}_4\|^2\xi^2}{\xi^2+\|\boldsymbol{s}_4\|^2} - c_3\xi\,\mathrm{sig}(\xi)^\gamma - c_4\xi\,\mathrm{sign}(\xi) \\
&\le -\boldsymbol{s}_4^{\mathrm{T}}\boldsymbol{s}_3 - k_4\boldsymbol{s}_4^{\mathrm{T}}\boldsymbol{s}_4 + \|\boldsymbol{s}_4\|\,\|\boldsymbol{d}_2\| + \lambda_3\boldsymbol{s}_4^{\mathrm{T}}\boldsymbol{v}_u - \frac{1}{2}\frac{\lambda_3^2\|\boldsymbol{s}_4\|^2\boldsymbol{s}_4^{\mathrm{T}}\boldsymbol{s}_4}{\xi^2+\|\boldsymbol{s}_4\|^2} + w_n^2\boldsymbol{s}_4^{\mathrm{T}}\Delta\boldsymbol{u} \\
&\quad - \frac{\boldsymbol{s}_4^{\mathrm{T}}\boldsymbol{s}_4}{4\varepsilon_2} - \lambda_1\boldsymbol{v}_u^{\mathrm{T}}\boldsymbol{v}_u - \left|w_n^2\boldsymbol{s}_4^{\mathrm{T}}\Delta\boldsymbol{u}\right| - \frac{1}{2}w_n^2\Delta\boldsymbol{u}^{\mathrm{T}}\Delta\boldsymbol{u} - w_n^2\boldsymbol{v}_u^{\mathrm{T}}\Delta\boldsymbol{u} - c_1\boldsymbol{v}_u^{\mathrm{T}}\mathrm{sig}(\boldsymbol{v}_u)^\gamma \\
&\quad - c_2\boldsymbol{v}_u^{\mathrm{T}}\mathrm{sign}(\boldsymbol{v}_u)\lambda_2\xi^2 - \frac{1}{2}\frac{\lambda_3^2\|\boldsymbol{s}_4\|^2\xi^2}{\xi^2+\|\boldsymbol{s}_4\|^2} - c_3\xi\,\mathrm{sig}(\xi)^\gamma - c_4\xi\,\mathrm{sign}(\xi) \\
&\quad + \ell_{2i}|s_{4i}| - \ell_{2i}s_{4i}\tan\left(\frac{s_{4i}}{p_2}\right) + \varsigma_2\tilde{\ell}_{2i}\hat{\ell}_{2i}
\end{aligned} \tag{41}$$

According to

$$\begin{aligned}
&-\ell_{2i}s_{4i}\tan\left(\frac{s_{4i}}{p_2}\right) \le -\frac{\ell_{2i}s_{4i}^2}{|s_{4i}|+p_2} \\
&\tilde{\ell}_{2i}\hat{\ell}_{2i} = \tilde{\ell}_{2i}\left(\ell_{2i}-\tilde{\ell}_{2i}\right) \le \frac{1}{2}\ell_{2i}^2 - \frac{1}{2}\tilde{\ell}_{2i}^2 \\
&\|\boldsymbol{s}_4\|\,\|\boldsymbol{d}_2\| \le \frac{\|\boldsymbol{s}_4\|^2}{4\varepsilon_2} + \varepsilon_2 h_2, \quad w_n^2\boldsymbol{s}_4^{\mathrm{T}}\Delta\boldsymbol{u} - \left|w_n^2\boldsymbol{s}_4^{\mathrm{T}}\Delta\boldsymbol{u}\right| \le 0 \\
&\lambda_3\boldsymbol{s}_4^{\mathrm{T}}\boldsymbol{v}_u - w_n^2\boldsymbol{v}_u^{\mathrm{T}}\Delta\boldsymbol{u} \le \frac{1}{2}\lambda_3\|\boldsymbol{s}_4\|^2 + \boldsymbol{v}_u^{\mathrm{T}}\boldsymbol{v}_u + \frac{1}{2}w_n^2\Delta\boldsymbol{u}^{\mathrm{T}}\Delta\boldsymbol{u} \\
&-\frac{1}{2}\frac{\lambda_3^2\|\boldsymbol{s}_4\|^2\boldsymbol{s}_4^{\mathrm{T}}\boldsymbol{s}_4}{\xi^2+\|\boldsymbol{s}_4\|^2} - \frac{1}{2}\frac{\lambda_3^2\|\boldsymbol{s}_4\|^2\xi^2}{\xi^2+\|\boldsymbol{s}_4\|^2} = -\frac{1}{2}\lambda_3^2\|\boldsymbol{s}_4\|^2
\end{aligned} \tag{42}$$

substituting (42) into (41), it can be simplified as

$$\begin{aligned}
\dot{V}_{13} \le &-\boldsymbol{s}_4^{\mathrm{T}}\boldsymbol{s}_3 - k_4\boldsymbol{s}_4^{\mathrm{T}}\boldsymbol{s}_4 + \varepsilon_2 h_2 + \ell_{2i}|s_{4i}| - \lambda_1\boldsymbol{v}_u^{\mathrm{T}}\boldsymbol{v}_u + \boldsymbol{v}_u^{\mathrm{T}}\boldsymbol{v}_u \\
&- c_1\boldsymbol{v}_u^{\mathrm{T}}\mathrm{sig}(\boldsymbol{v}_u)^\gamma - \frac{\ell_{2i}s_{4i}^2}{|s_{4i}|+p_2} + \frac{\varsigma_2}{2}\ell_{2i}^2 - \frac{\varsigma_2}{2}\tilde{\ell}_{2i}^2 \\
&- c_2\boldsymbol{v}_u^{\mathrm{T}}\mathrm{sign}(\boldsymbol{v}_u)\lambda_2\xi^2 - \lambda_2\xi^2 - c_2\xi\,\mathrm{sig}(\xi)^\gamma - c_4\xi\,\mathrm{sign}(\xi) \\
\le &-\boldsymbol{s}_4^{\mathrm{T}}\boldsymbol{s}_3 - k_4\boldsymbol{s}_4^{\mathrm{T}}\boldsymbol{s}_4 + \varepsilon_2 h_2 - (\lambda_1-1)\boldsymbol{v}_u^{\mathrm{T}}\boldsymbol{v}_u - c_2\boldsymbol{v}_u^{\mathrm{T}}\mathrm{sign}(\boldsymbol{v}_u)\lambda_2\xi^2 \\
&- \lambda_2\xi^2 - c_2\xi\,\mathrm{sig}(\xi)^\gamma - c_4\xi\,\mathrm{sign}(\xi) - \frac{\varsigma_2}{2}\tilde{\ell}_{2i}^2 + \frac{\varsigma_2}{2}\ell_{2i}^2
\end{aligned} \tag{43}$$

where $h_2 = d_{2M}^2$.

Based on (38), (41) and (43), the time derivative of V_1 is

$$\begin{aligned}\dot{V}_1 \leq & -k_2\boldsymbol{s}_2^{\mathrm{T}}\boldsymbol{s}_2+\varepsilon_1 h_1-k_3\boldsymbol{s}_3^{\mathrm{T}}\boldsymbol{s}_3-k_4\boldsymbol{s}_4^{\mathrm{T}}\boldsymbol{s}_4+\varepsilon_2 h_2-\frac{\varsigma_1}{2}\tilde{\ell}_{1i}^2+\frac{\varsigma_1}{2}\ell_{1i}^2-\frac{\varsigma_2}{2}\tilde{\ell}_{2i}^2+\frac{\varsigma_2}{2}\ell_{2i}^2\\ & -(\lambda_1-1)\boldsymbol{v}_u^{\mathrm{T}}\boldsymbol{v}_u-c_1\boldsymbol{v}_u^{\mathrm{T}}\mathrm{sig}(\boldsymbol{v}_u)^\gamma-\lambda_2\xi^2-c_2\xi\mathrm{sig}(\xi)^\gamma\\ \leq & -k_2\boldsymbol{s}_2^{\mathrm{T}}\boldsymbol{s}_2-\left(k_3-\frac{1}{2}\right)\boldsymbol{s}_3^{\mathrm{T}}\boldsymbol{s}_3-\left(k_4-\frac{1}{2}\right)\boldsymbol{s}_4^{\mathrm{T}}\boldsymbol{s}_4-\frac{\varsigma_1}{2}\tilde{\ell}_{1i}^2-\frac{\varsigma_2}{2}\tilde{\ell}_{2i}^2\\ & -(\lambda_1-1)\boldsymbol{v}_u^{\mathrm{T}}\boldsymbol{v}_u-\lambda_2\xi^2+\varepsilon_1 h_1+\varepsilon_2 h_2+\frac{\varsigma_1}{2}\ell_{1i}^2+\frac{\varsigma_2}{2}\ell_{2i}^2\\ \leq & -\varphi V_1+\rho\end{aligned} \tag{44}$$

where

$$\begin{aligned}&\varphi=\min\left\{2k_2,2\left(k_3-\frac{1}{2}\right),2\left(k_4-\frac{1}{2}\right),2(\lambda_1-1),\varsigma_1\beta_1,\varsigma_2\beta_2,2\lambda_2\right\}\\ &\rho=\varepsilon_1 h_1+\varepsilon_2 h_2+\frac{\lambda_1}{2}\ell_{1i}^2+\frac{1}{2}\ell_{2i}^2\end{aligned} \tag{45}$$

The $e^{\varphi t}$ multiplies both sides of Equation (44)

$$\left(V_1(t)+\varphi V_1(t)\right)e^{\varphi t}\leq\rho e^{\varphi t} \tag{46}$$

Integrate (46) and we can obtain

$$V_1(t)\leq\left(V_1(0)-\Gamma\right)e^{-\varphi t}+\Gamma \tag{47}$$

where $\Gamma=\rho/\varphi$.

From (33), it can be obtained as

$$\frac{1}{2}\boldsymbol{s}_i^T\boldsymbol{s}_i\leq V_1(t)\leq V_1(0)+\Gamma \tag{48}$$

Further

$$\|\boldsymbol{s}_i\|\leq\sqrt{V_1(0)+\Gamma}=\Delta_i\quad(i=1,2) \tag{49}$$

Thus, the $\boldsymbol{s}_i$ converges to the region Δ_i in finite time.

The conclusion (1) shows that $\boldsymbol{s}_i$ will converge to the region Δ_i, and then the x_{1i} and x_{2i} of convergence are analyzed as follows.

Case 1: if $|x_{1i}|\leq\eta$, the x_{1i} is already converged to the region $|x_{1i}|\leq\Delta_{x_{1i}}$ in finite time, and based on (10), it can be written as

$$s_{2i}=x_{2i}+\frac{\alpha_1+\alpha_2 r_1}{\alpha_0}\left(\exp(\alpha_0|x_{1i}|)-1\right)\mathrm{sign}\left(x_{1i}\right)+\alpha_2 r_2\mathrm{sign}\left(x_{1i}\right)\left(x_{1i}\right)^2,\ i=1,2 \tag{50}$$

Thus

$$|x_{2i}|\leq\frac{\alpha_1+\alpha_2 r_1}{\alpha_0}\left(\exp(\alpha_0\eta)-1\right)+\alpha_2 r_2\eta^2+\Delta_i \tag{51}$$

Case 2: if $|x_{1i}|>\eta$, based on (10), it can be written as

$$x_{2i}+\frac{\alpha_1}{\alpha_0}\left(\exp(\alpha_0|x_{1i}|)-1\right)\mathrm{sign}\left(x_{1i}\right)+\alpha_2\mathrm{sig}\left(x_{1i}\right)^\gamma=\Delta\varpi_i \tag{52}$$

where $\Delta\varpi_i\leq\Delta_i$.

According to (52), it can be divided into two forms as follows

$$x_{2i}+\left(\alpha_1-\frac{\alpha_0\Delta\varpi_i}{T\left(x_{1i}\right)}\right)\frac{T\left(x_{1i}\right)}{\alpha_0}+\alpha_2\mathrm{sig}\left(x_{1i}\right)^\gamma=0 \tag{53}$$

$$x_{2i}+\frac{\alpha_1 T\left(x_{1i}\right)}{\alpha_0}+\left(\alpha_2-\frac{\Delta\varpi_i}{\mathrm{sig}\left(x_{1i}\right)^\gamma x_{1i}}\right)\mathrm{sig}\left(x_{1i}\right)^\gamma=0 \tag{54}$$

where $T(x_{1i}) = (\exp(\alpha_0 |x_{1i}|) - 1)\,\mathrm{sgn}(x_{1i})$, and according to (53), the following inequalities can be obtained as

$$\alpha_1 - \frac{\alpha_0 \Delta\varpi_i}{T(x_{1i})} > 0 \tag{55}$$

From (55), it can be obtained that the x_{1i} can satisfy the inequality as

$$|x_{1i}| \leq \frac{1}{\alpha_0} \ln \frac{\alpha_0 \Delta_i + \alpha_1}{\alpha_1} \tag{56}$$

From (54), inequality is satisfied as follows

$$\alpha_2 - \frac{\Delta\varpi_i}{\mathrm{sig}(x_{1i})^{\gamma} x_{1i}} > 0 \tag{57}$$

By similar analysis, it can be obtained that the x_{1i} converges to the region in finite time.

$$|x_{1i}| \leq \left(\frac{\Delta\varpi_i}{\alpha_2}\right)^{\gamma} \leq \left(\frac{\Delta_i}{\alpha_2}\right)^{\gamma} \tag{58}$$

Therefore, x_{1i} can converge to the region in finite time

$$|x_{1i}| \leq \Delta x_{1i} = \max\left\{\eta, \min\left\{\frac{1}{\alpha_0} \ln \frac{\alpha_0 \Delta_i + \alpha_1}{\alpha_1}, \left(\frac{\Delta_i}{\alpha_2}\right)^{\gamma}\right\}\right\} \tag{59}$$

According to (52) and (59), it can be got that x_{2i} converges to the region in finite time

$$\begin{aligned} x_{2i} &\leq \Delta\varpi - \frac{\alpha_1}{\alpha_0}(\exp(\alpha_0 |x_{1i}|) - 1)\,\mathrm{sign}(x_{1i}) + \alpha_2 \mathrm{sig}(x_{1i})^{\gamma} \\ &\leq \Delta x_{1i} + \frac{\alpha_1}{\alpha_0}(\exp(\alpha_0 \Delta x_{1i}) - 1) + \alpha_2 \mathrm{sig}(\Delta x_{1i})^{\gamma} = \Delta x_{2i} \end{aligned} \tag{60}$$

Therefore, the $\boldsymbol{x}_1$ and $\boldsymbol{x}_2$ can converge to the region $|x_{1i}| \leq \Delta_{x_{1i}}$ and $|x_{2i}| \leq \Delta_{x_{2i}}$ in finite time. Theorem 3.1 is proved.

Remark 3.1. *In guidance law (27), we introduce $\lambda_3 \boldsymbol{v}_u$ to deal with the input constraints of guidance system, mainly for the following two conditions.*

When $\|\boldsymbol{v}_u\| \geq \eta_1$, there is an input constraint in control system

(a) When $u_i \geq u_M$, $\lambda_3 \boldsymbol{v}_u$ can guarantee that u_i reduces to $u_i = u_M$.

(b) When $u_i \leq -u_M$, $\lambda_3 \boldsymbol{v}_u$ can guarantee that u_i increases to $u_i = -u_M$.

Thus, $u_i = u_M$ or $u_i = -u_M$.

When $\|\boldsymbol{v}_u\| < \eta_1$, there are no input constraints in guidance system, that is to say $\Delta u_i = 0$, the $\lambda_3 \boldsymbol{v}_u$ can guarantee that u_{Vc} satisfies $-u_M < u_i < u_M$. Thus $u_i = \mathrm{sat}(u_i)$.

4. **Numerical Examples.** To demonstrate the effectiveness of the designed guidance law (27), numerical examples are presented in the section. Referring to [11], the simulation parameters are as follows: the mission parameters: (1) velocity: $V_M = 1500$ m/s; (2) initial position coordinates: $x_M(0) = 0$ km, $y_M(0) = 0$ km, and $z_M(0) = 0$ km; (3) initial heading angle and flight path angle: $\varphi_M(0) = -30$ deg and $\theta_M(0) = 30$ deg. The target parameters: (1) velocity: $V_{\mathrm{T}} = 900$ m/s; (2) initial position coordinates: $x_t(0) = 4.32$ km, $y_t(0) = 6.84$ km, and $z_t(0) = 11.046$ km; (3) initial heading angle and flight path angle: $\varphi_{\mathrm{T}}(0) = 140$ deg and $\theta_{\mathrm{T}}(0) = -10$ deg. Among the parameters above, the maximal acceleration of the missile is $40g$ that is the acceleration of gravity ($g = 9.8$ m/s^2). The desired LOS flight path angle is $q_d = -21.1$ deg and the LOS is $q_d = -37.1$ deg.

In order to test the robustness to the proposed guidance strategy, we have added a comparison with command filter back-stepping guidance law (CFBG) [23]. The parameter uncertainties of the missile model are given as $d_\varepsilon = 100 \sin t$ m/s^2 and $d_\beta = 100 \sin t$ m/s^2, and the simulation is divided into two kinds of target accelerations as follows.

Case 1: $a_{\mathrm{T}\varepsilon} = 7g\sin(t)$ and $a_{\mathrm{T}\beta} = 7g\sin(t)$.
Case 2: $a_{\mathrm{T}\varepsilon} = 7g$ and $a_{\mathrm{T}\beta} = 7g$.
(1) Simulation analysis for consine maneuvering.

The parameters about the second-order dynamics of missile autopilot are given as $\zeta = 0.8$ and $\omega_n = 10$ rad/s. The parameters of guidance law (27) are chosen as $\alpha_0 = 0.5$, $\alpha_1 = 1.5$, $\alpha_2 = 4.5$, $\eta = \eta_1 = \eta_2 = 0.02$, $\varepsilon_1 = 0.05$, $\varepsilon_2 = 0.05$, $k_1 = 1.2$, $k_2 = 2.5$, $k_3 = 10$, $k_4 = 3.5$, $\lambda = 0.75$, $\lambda_1 = 0.5$, $\lambda_2 = 1.2$, $\lambda_3 = 1.35$, $\varsigma_{111} = \varsigma_{112} = 1.5$, $\varsigma_{101} = \varsigma_{102} = 2$, $\mu_{101} = \mu_{102} = 2$, $\mu_{111} = \mu_{112} = 2.5$, $p_1 = p_2 = 0.01$, $\beta_1 = 0.05$, $\varsigma_1 = 0.1$, $\varsigma_{211} = \varsigma_{212} = 1.5$, $\varsigma_{201} = \varsigma_{202} = 2$, $\mu_{201} = \mu_{202} = 2$, $\mu_{211} = \mu_{212} = 2.5$, $c_1 = c_2 = 1.25$, $c_3 = c_4 = 1.55$, $\beta_2 = 0.05$, $\varsigma_2 = 0.1$. For case 1, the simulation curves of the missile-target are shown in Figures 2(a)-2(g). Table 1 presents the miss distances for two cases, and also reveals interception times.

Table 1. Miss distances and interception times for the two cases

Guidance laws	Case 1		Case 2	
	Miss distance (m)	Interception time (s)	Miss distance (m)	Interception time (s)
Proposed method	0.715	8.587	0.345	9.529
CFBG	1.455	8.532	1.860	9.480

From Figures 2(a) and 2(b), the LOS angular rates $\dot{q}_\varepsilon$ and $\dot{q}_\beta$ converging to zero in finite time can be ensured by both guidance laws for case 1. However, the convergence property under the proposed method has smoother and smaller chattering than the CFBG.

From Table 1, it can be observed that the miss distance under the designed guidance laws is similar to that under the CFBG for case 1. From Figures 2(c) and 2(d), assuredly, the LOS angles q_ε and q_β under the presented law can also converge to their desired terminal LOS angles respectively. However, the CFBG law cannot consider the impact angle constraints during the design process of guidance law. Figures 2(e) and 2(f) depict the missile lateral accelerations under the two guidance laws for case 1, which makes the proposed control laws be possible for the actual physical limit. However, the proposed method is continuous, smooth and has small control amplitude compared with CFBG. It can be visibly observed from Figures 2(g) and 2(h) that the proposed law can guarantee guidance performance about the maneuvering target intercepted by the missile.

(2) Simulation analysis for constant maneuvering

For case 2, its control parameters are the same as case 1. The simulation curves obtained by the proposed method and CFBG are shown in Figures 3(a)-3(g) for case 2. The simulation curves include the responses of line of sight angle, line of sight angular rate, missile acceleration command, relative distance, trajectories of the missile and the target. From Figures 3(a) and 3(b), assuredly the performance of the designed guidance laws is superior in comparison with CFBG because it can drive the LOS angular rate to zero faster. The miss distance is 0.345 m about the proposed guidance law while CFBG law is 1.860 m. The curves of LOS angle error under the presented method and CFBG are shown in Figures 3(c) and 3(d). Assuredly, the proposed method can make LOS angles converge to their desired terminal LOS angles. Form Figures 3(e) and 3(f), it can be known that the missile accelerations under both proposed guidance law can satisfy the reasonable bounds. However, the missile accelerations produced by the presented method is much smoother and smaller than those under the CFBG. According to the observation from Figures 3(g)-3(h), the missile precision intercepting the maneuvering target can be guaranteed under the proposed method.

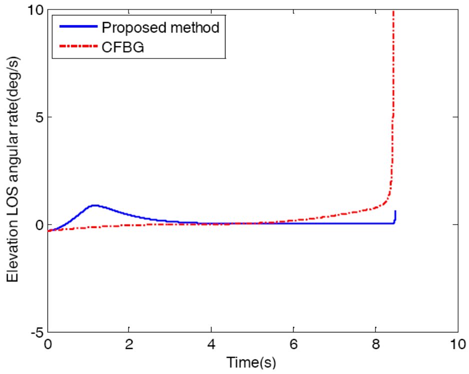

(a) Elevation line of sight angular rate

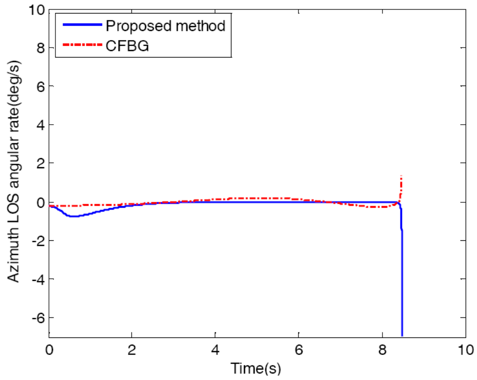

(b) Azimuth line of sight angular rate

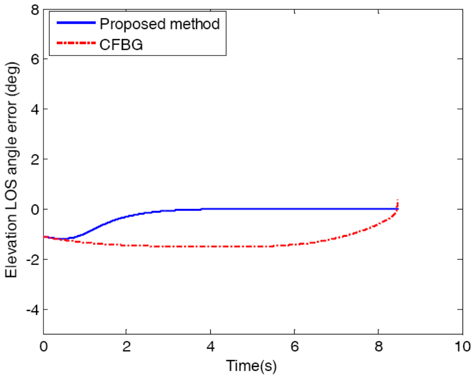

(c) Elevation line of sight angle error

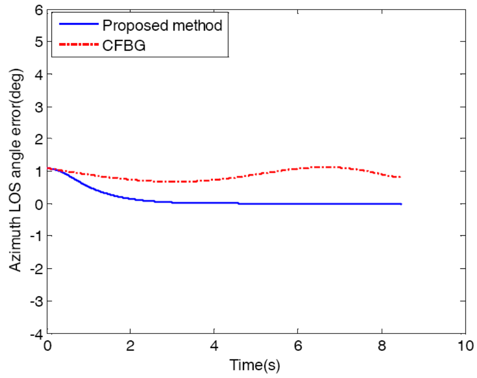

(d) Azimuth line of sight angle error

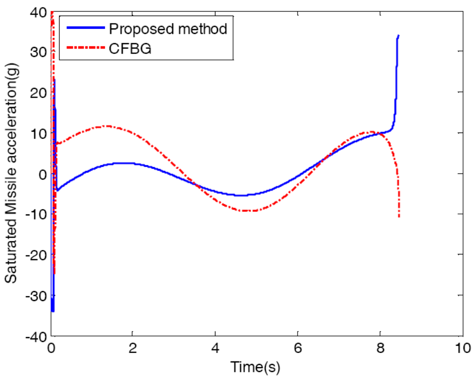

(e) Elevation acceleration command in loop

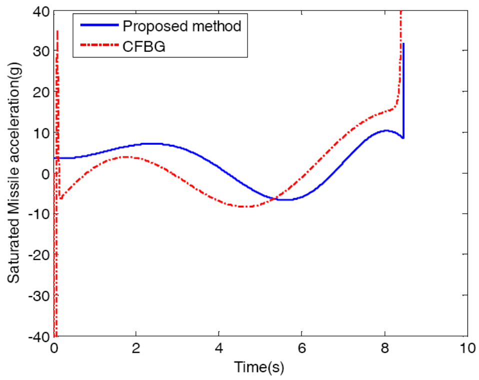

(f) Azimuth acceleration command

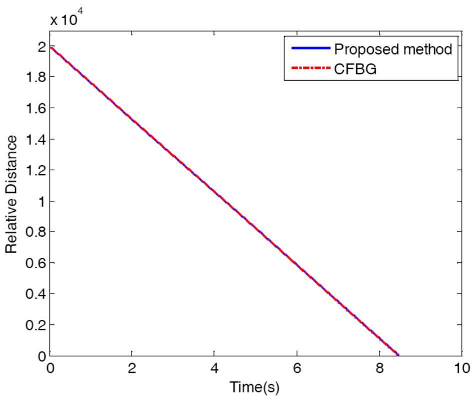

(g) Relative distance

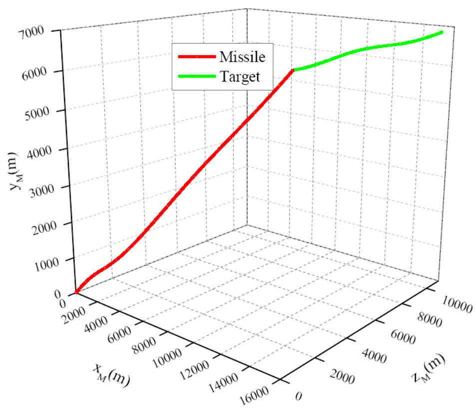

(h) Interception geometry

FIGURE 2. Simulation results for case 1

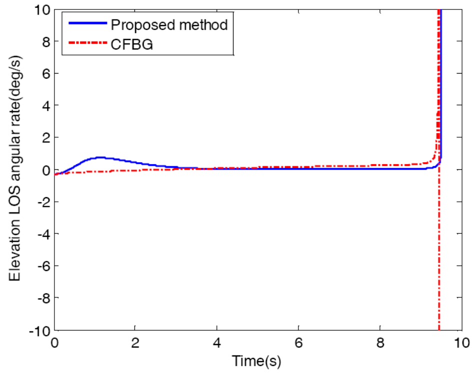

(a) Elevation line of sight angular rate

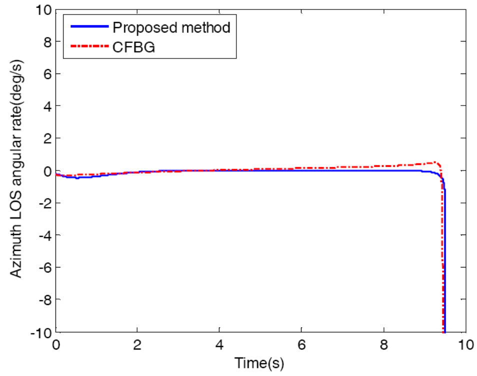

(b) Azimuth line of sight angular rate

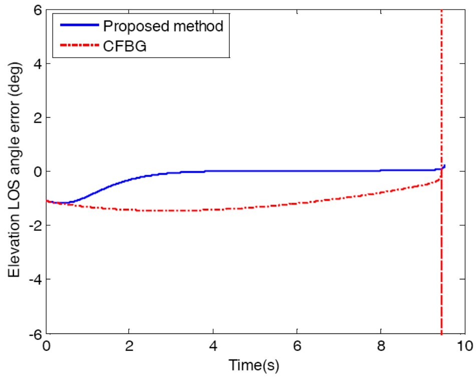

(c) Elevation line of sight angle error

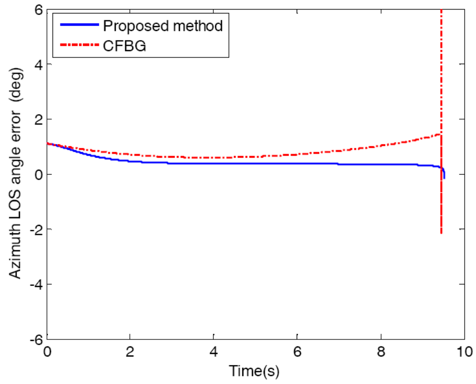

(d) Azimuth line of sight angle error

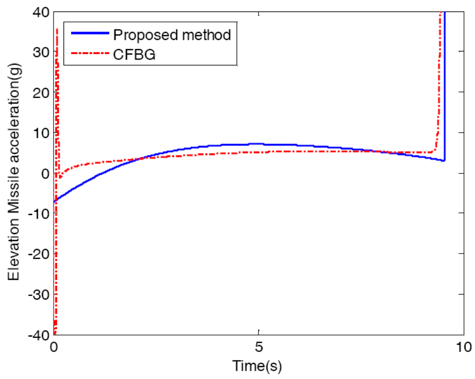

(e) Elevation acceleration command

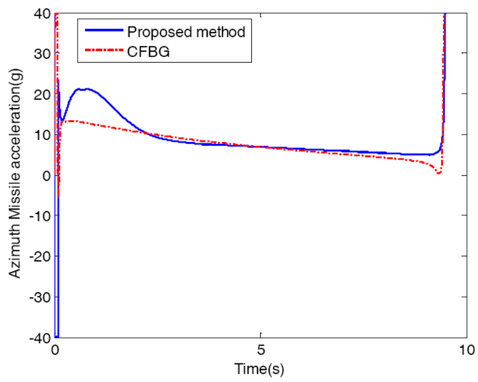

(f) Azimuth acceleration command

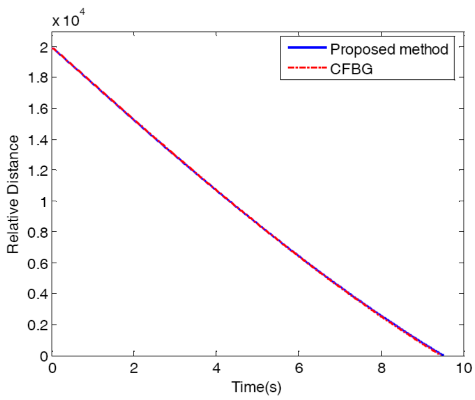

(g) Relative distance

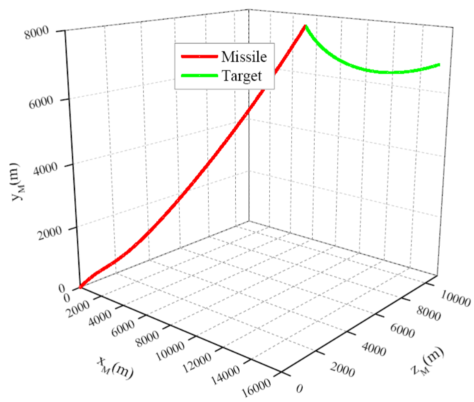

(h) Interception geometry

FIGURE 3. Simulation results for case 2

5. **Conclusions.** In this paper, a new adaptive dynamic surface guidance scheme is proposed for the terminal guidance problem of missiles intercepting the maneuvering targets subject to impact angle constraints, second-order dynamics of missile autopilot and input constraints. The conclusions are as the following.

(1) The proposed guidance law employs the sliding mode filter to eliminate the "explosion of complexity" in inherent in traditional back-stepping method. At the same time, the adaptive algorithms are introduced to eliminate the effect of the error caused by the sliding mode filter.

(2) The auxiliary system is introduced in controller design to solve input constraints, which makes the designed controller meet physical constraints of the actuators. And under the designed controller, the states of guidance system can be stabilized in a small region around zero in finite time.

(3) The simulation results demonstrate that the guidance scheme is effective for the missiles to intercept the maneuvering targets in different situations.

(4) In the future, the problem of actuator faults and some states unknown should be considered in the guidance law design. Under the constraints above, how to develop the advance guidance law which can produce higher guidance precision and better robustness is a great difficult problem.

Acknowledgment. The authors would like to acknowledge the financial support provided by the Harbin Municipal Science and Technology Bureau Project (2017RAQXJ133) Supported by Harbin Foundation for Youths (2017RAQXJ137).

REFERENCES

[1] S. Sentilles, P. Štěpán and J. Carlson, Integration of extra-functional properties in component models, *Component-Based Software Engineering*, pp.173-190, 2009.
[2] A. Ratnoo and D. Ghose, Impact angle constrained interception of stationary targets, *Journal of Guidance, Control, and Dynamics*, vol.1, no.6, pp.1816-1821, 2008.
[3] B. S. Kim, J. G. Lee and H. S. Han, Biased PNC law for impact with angular constraint, *IEEE Trans. Aerospace and Electronic Systems*, vol.34, no.1, pp.277-288, 1998.
[4] M. G. Yoon, Relative circular navigation guidance for the impact angle control problem, *IEEE Trans. Aerospace and Electronic Systems*, vol.44, no.4, pp.1449-1463, 2008.
[5] M. G. Yoon, Relative circular navigation guidance for three-dimensional impact angle control problem, *Journal of Aerospace Engineering*, vol.23, no.4, pp.300-308, 2010.
[6] C. Liu, Z.-J. Zou and J.-C. Yin, Path following and stabilization of underactuated surface vessels based on adaptive hierarchical sliding mode, *International Journal of Innovative Computing, Information and Control*, vol.10, no.3, pp.909-918, 2014.
[7] H. Liu, X. Shi, X. Bi and J. Zhang, Backstepping-based terminal sliding mode control for rendezvous and docking with a tumbling spacecraft, *International Journal of Innovative Computing, Information and Control*, vol.12, no.3, pp.929-940, 2016.
[8] J. Song, S. Song, Y. Guo and H. Zhou, Nonlinear disturbance observer-based fast terminal sliding mode guidance law with impact angle constraints, *International Journal of Innovative Computing, Information and Control*, vol.11, no.3, pp.787-802, 2015.
[9] S. R. Kumar, S. Rao and D. Ghose, Sliding-mode guidance and control for all-aspect interceptors with terminal angle constraints, *Journal of Guidance, Control, and Dynamics*, vol.35, no.4, pp.1230-1246, 2012.
[10] D. Zhou, Y. A. Zhang and G. R. Duan, Multiple model adaptive two-step filter and motion tracking sliding-mode guidance for missiles with time lag in acceleration, *Transactions of the Japan Society for Aeronautical and Space Sciences*, vol.47, no.156, pp.81-89, 2004.
[11] P. P. Qu and D. Zhou, Three-dimensional guidance law accounting for second-order dynamics of missile autopilot, *Chinese Journal of Aeronautics*, vol.32, no.11, pp.2096-2105, 2011.
[12] P. P. Qu and D. Zhou, A dimension reduction observer-based guidance law accounting for dynamics of missile autopilot, *Proc. of the Institution of Mechanical Engineers, Part G: Journal of Aerospace Engineering*, vol.227, no.7, pp.1114-1121, 2013.

[13] S. M. He, D. F. Lin and J. Wang, Robust terminal angle constraint guidance law with autopilot lag for intercepting maneuvering targets, *Nonlinear Dynamics*, vol.1, no.81, pp.881-892, 2015.

[14] G. Hexner, T. Shima and H. Weiss, LQC guidance law with bounded acceleration command, *IEEE Trans. Aerospace and Electronic Systems*, vol.44, no.1, pp.77-86, 2008.

[15] M. Chen, S. S. Ge and B. Ren, Adaptive tracking control of uncertain MIMO nonlinear systems with input constraints, *Automatica*, vol.47, no.3, pp.452-465, 2011.

[16] M. Zhang, X. Shen and T. Li, Fault tolerant attitude control for cubesats with input saturation based on dynamic adaptive neural network, *International Journal of Innovative Computing, Information and Control*, vol.12, no.2, pp.651-663, 2016.

[17] Y. J. Si, S. M. Song and X. Q. Wei, An adaptive reaching law based three-dimensional guidance laws for intercepting hypersonic vehicle, *International Journal of Innovative Computing, Information and Control*, vol.13, no.4, pp.1335-1349, 2017.

[18] D. Zhou and B. Xu, Adaptive dynamic surface guidance law with input saturation constraint and autopilot dynamics, *Journal of Guidance, Control, and Dynamics*, vol.39, no.55, pp.1155-1162, 2016.

[19] B. Xu and D. Zhou, Three dimensional adaptive dynamic surface guidance law accounting for autopilot lag, *American Control Conference (ACC)*, pp.578-583, 2014.

[20] X. Liang, M. Hou and G. Duan, Integrated guidance and control for missile in the presence of input saturation and angular constraints, *The 32nd Chinese Control Conference (CCC)*, pp.1070-1075, 2013.

[21] W. Wang, S. Xiong and S. Wang, Three dimensional impact angle constrained integrated guidance and control for missiles with input saturation and actuator failure, *Aerospace Science and Technology*, vol.53, pp.169-187, 2016.

[22] S. Sheng, D. Zhou and W. T. Hou, A guidance law with finite time convergence accounting for autopilot lag, *Aerospace Science and Technology*, vol.25, pp.132-137, 2013.

[23] R. Du, K. Meng and D. Zhou, Design of three-dimensional nonlinear guidance law with bounded acceleration command, *Aerospace Science and Technology*, vol.46, pp.168-175, 2015.

[24] M. Chen and S. S. Ge, Adaptive neural output feedback control of uncertain nonlinear systems with unknown hysteresis using disturbance observer, *IEEE Trans. Industrial Electronics*, vol.62, no.12, pp.7706-7716, 2015.

[25] J. H. Song and S. M. Song, Robust impact angle constraints guidance law with autopilot lag and acceleration saturation consideration, *Transactions of the Institute of Measurement and Control*, 2018.